www.sciencetranslationalmedicine.org/cgi/content/full/5/179/179ra47/DC1

Supplementary Materials for

Inertial Focusing for Tumor Antigen–Dependent and –Independent Sorting of Rare Circulating Tumor Cells

Emre Ozkumur, Ajay M. Shah, Jordan C. Ciciliano, Benjamin L. Emmink, David T. Miyamoto, Elena Brachtel, Min Yu, Pin-i Chen, Bailey Morgan, Julie Trautwein, Anya Kimura, Sudarshana Sengupta, Shannon L. Stott, Nezihi Murat Karabacak, Thomas A. Barber, John R. Walsh, Kyle Smith, Philipp S. Spuhler, James P. Sullivan, Richard J. Lee, David T. Ting, Xi Luo, Alice T. Shaw, Aditya Bardia, Lecia V. Sequist, David N. Louis, Shyamala Maheswaran, Ravi Kapur, Daniel A. Haber, Mehmet Toner*

*Corresponding author. E-mail: mtoner@hms.harvard.edu

Published 3 April 2013, *Sci. Transl. Med.* **5**, 179ra47 (2013)
DOI: 10.1126/scitranslmed.3005616

The PDF file includes:

Supplementary Materials and Methods

Cell culture

MDA-MB-231, SKBR3, and MCF10A cell lines were obtained from ATCC (Manassas, VA), PC3-9 cells were obtained from Veridex, LLC, and LBX1-expressing MCF10A cells were derived from a stable cell line previously developed and published by our laboratory. All cells were cultured and propagated in accordance with providers recommendations and maintained in humid, 37°C, 5% CO_2 cell culture incubators. As noted for specific experiments, cells were prelabeled with a fluorescent tracer dye (CellTracker Red or CellTracker Green, Life Technologies) following the manufacturer's recommended protocol.

Fluorescent microscopy

All fluorescent microscopy was conducted using either inverted or upright microscopes (TiE or Eclipse 90i, Nikon) with the appropriate filter cubes for the respective stains. For scanning of immunofluorescent stained and plated cells, an automated system (BioView) was used.

Debulking array characterization

To characterize the performance of the two array designs (fig. S3), whole-blood samples (n > 10) were processed through each chip, and the starting blood as well as outlet product and waste solutions were analyzed to quantify nucleated cell retention, RBC removal and platelet removal. Analysis was conducted using a Sysmex KX blood analyzer, or for dilute

solutions, by staining nucleated cells with Hoescht dye and determining their concentration using a Nageotte chamber. Dilute RBC concentrations were determined by counting all events in brightfield and subtracting the number of nucleated events detected using the Hoescht stain.

Evaluating critical variables on cell focusing using streak quality

To characterize the effects of critical variables on cell focusing, solutions with various concentrations of WBCs and RBCs were prepared by initially debulking the whole blood and labeling the WBCs with calceinAM (1 μM). Samples were then diluted to achieve the desired concentrations and RBCs were added as needed to achieve the desired hematocrit. They were then processed through the inertial focusing chip and imaged at 10x using long exposure times (~5 seconds) to collect a fluorescent streak image that represents the position of >1000 individual events at the end of the deflection region. A line-cut across the image is taken and signal intensity across the channel was measured. Commercially available curve fitting tools (Matlab, Mathworks) were used to determine the full-width-half-maximum (FWHM) of the streak image, and streak quality was defined as (Channel Width / FWHM); the tighter the focus stream, the smaller the FWHM, the greater the streak quality (fig. S4).

Experiments for optimization of magnetic labeling

Prior to integrated CTC-iChip spiked cell isolation experiments, optimization of labeling efficiencies were conducted (fig. S2). For positive selection, pre-stained cell lines with low and high EpCAM expression were spiked into whole blood, incubated with various amounts

of anti-EpCAM coated beads, and samples were mixed using either active magnetic mixing or passive mixing. Following mixing, samples were processed through a debulking array to remove RBCs and collected in a 24-well plate; target cells were identified based on their fluorescence and their bead loading was evaluated. For negative depletion, whole blood samples were passively incubated for 60 minutes with various combinations of anti-CD45 and anti-CD15 coated beads. Samples were then RBC lysed (BioLegend 420301, per manufacturer's protocols) and stained with Hoescht dye to accurately identify nucleated cells. Of note, RBC lysis was used only to generate fig. S2B, and microfluidic RBC removal was applied for rest of the presented study.

Bead loading was evaluated on more than 100 nucleated events in each sample. In passive mixing, the samples underwent end-over-end rotation for 15 minutes (positive selection) or 60 minutes (negative depletion). In this experiment, the number of beads added was normalized to WBC concentration; this approach was used for all negative depletion experiments, however a fixed magnetic bead concentration was used for the positive selection experiments.

Quantitative modeling of magnetophoretic cell deflection

The deflection channel is 500 μm wide, providing cells with a residence time of τ_r ~600 ms at the bulk flow rate of 100 μl/min (with fluid velocity ~60 mm/s). Finite element modeling of the quadrapole magnetic circuit (fig. S5) was conducted using commercially available software (COMSOL). Second order magnetic effects due to position in the z-dimension or edge effects at the beginning or end of the deflection region (y-dimension) were not considered. Model yields an estimate 0.22 T magnetic field strength, and 150 T/m

as the magnetic field gradient (dB/dx) across the channel. At this field strength, magnetization of Dynal MyONE beads saturate. With saturated magnetic beads, the magnetic force on each bead can be calculated by equation S1:

$$F_{mag} = \mu_0 V M_s \frac{\partial H_x}{\partial x} \qquad (S1)$$

where μ_0 is the permeability of the free space, V is the volume of a single magnetic particle, and M_s is the volume magnetic saturation of a single bead. The speed that cells can deflect towards the collection wall is calculated through balancing the magnetic force with the counter acting drag force (eqn. S2):

$$F_{mag} = N\mu_0 V M_s \frac{\partial H_x}{\partial x} = F_{drag} = 6\pi\eta r u_x \qquad (S2)$$

where η is the fluid (water) viscosity, r is cell radius, and u_x is the speed of deflection. Notice that, total magnetic force on the cell is multiplied by the number of beads on the cell, N. Note that u_x is the speed of magnetically deflecting cells, in the direction perpendicular to fluid flow; however, cells have finite amount of time to deflect until they arrive the end of the channel (4 cm) while traveling in "y" direction with the speed of U_y. U_y is calculated using the fluid velocity profile. The fluid velocity profile in the deflection region was calculated (eqn. S3) by solving the Navier-Stokes equation with the associated boundary conditions of the channel, given the bulk-average flow rate and channel dimensions:

$$\left(\frac{\partial^2}{\partial x^2} + \frac{\partial^2}{\partial y^2}\right)\mathbf{u} = -\frac{\Delta p}{\eta L}, \text{ for } -250\mu m < y < 250\mu m \; and \; 0 < z < 50\mu m \qquad (S3)$$

Here, $\mathbf{u}$ is the velocity, Δp is pressure difference, η is for viscosity. w, h, L are the width height and length of the channel, and x, y, and z are the coordinates used for modeling. Solution of this equation for high aspect ratio channels, where $\alpha = h/w \rightarrow 0$ (in this case α = 50 μm/500 μm = 0.1), is estimated as follows in eqn. S4:

$$u(y,z) \approx \frac{48\alpha Q}{\pi^3 h^2 (1-0.63\alpha)} \sum_{n,odd}^{\infty} \frac{1}{n^3} \left[1 - \frac{\cosh\left(n\pi\frac{y}{h}\right)}{\cosh\left(n\pi\frac{w}{2h}\right)}\right] \sin\left(n\pi\frac{z}{h}\right) \qquad (S4)$$

where Q is the volumetric flow rate. This equation gives the longitudinal speed, u_y, of a cell at any cross section in the channel. u_x is derived from eqn. S2. The initial coordinates of a cell's position (x, y, and z) are empirically determined based on the position of a focused cell at the beginning of the magnetophoresis channel.

The model was processed in Matlab (Mathworks) and cell trajectories were estimated. The model's outcome was experimentally validated by preparing samples spiked with PC3-9 cells with a spectrum of bead labeling; these samples were then processed through the chip at various flow rates and bead loading on PC3-9 cells recovered in the deflected and undeflected solutions was quantified. Curve fits were applied to these distributions, and the intersection of the deflected and undeflected distributions was taken to represent the "minimum magnetic load needed for deflection" or "magnetic sensitivity" (Fig. 2; fig. S6)

Evaluation of EpCAM expression of cell lines

Five cell lines with a wide range of EpCAM expression were used to evaluate rare cell enrichment efficiency in the integrated system. EpCAM expression levels were measured using flow cytometry. Briefly, pure populations of each cell line were prepared in suspension, stained with either the biotinylated goat anti-EpCAM antibody or a biotinylated goat irrelevant IgG, rinsed, and labeled with a fluorescent avidin secondary stain. After labeling, the samples were rinsed, fixed, and evaluated using standard single-color flow cytometry (MACSQuant, MiltenyiBiotec). Analysis was conducting using

commercial flow cytometry software (FlowJo) and the median fluorescence value for each EpCAM-stained cell population was compared to the respective IgG control.

Lysis and RT-PCR

IFD products were put on DynaMag-2 Magnet for 5 minutes. Supernatants were discarded and bead- bound cells were lysed in RLT buffer (RNeasy Micro Kit, Qiagen). Cell lysates were flash frozen in liquid nitrogen and stored at -80°C. RNA isolation was done using RNeasy Micro Kit (Qiagen) according to manufacturer's instructions- the only exception was omission of treatment of column bound samples with DNAse. Isolated RNA was eluted in a small volume of RNAse-free water, and quantified using a NanoDrop 1000.

After RNA isolation, reverse transcription of RNA to cDNA using oligo dT was performed with SuperScript III First-Strand Synthesis System for RT-PCR (Invitrogen). For detection of *EML4-ALK* fusion cDNAs, partial nested PCR analysis was done with FideliTaq PCR Master Mix (Affymetrix). The forward primer was EML4.13F 5'- GTG CAG TGT TTA GCA TTC TTG GGG -3' and the reverse primers were ALK.20R.PCR I 5'- ACC TCC TTC AGG TCA CTG ATG G-3', ALK.20R 5'- TCT TGC CAG CAA AGG AGT AGT TGG-3'. During the first round of *EML4-ALK* amplification the samples were incubated at 95°C for 3 min and then subjected to 40 cycles of denaturation at 95°C for 30 s, annealing at 56°C for 30 s and polymerization at 72°C for 1 min. An aliquot of the product of first round of *EML4-ALK* amplification was taken for the second round of amplification, for which the samples were incubated at 95°C for 3 min and then subjected to 40 cycles of denaturation at 95°C for 30 s, annealing at 58°C for 30 s and polymerization at 72°C for 1 min. The amplification primers were synthesized by Invitrogen Custom DNA Oligos. PCR amplification was

performed in a thermocycler (Peltier ThermoCycler, MJ Research). Gel electrophoresis was done with an aliquot of RT- PCR products.

Sequencing of PCR products

The amplified *EML4-ALK* products were sequenced by the MGH DNA Core Facility, and results were analyzed with the ABI PRISM DNA sequence analysis software.

Cytology

The negative depletion product isolated from the whole blood of 12 patients with breast carcinomas [ER^+/PR^+ (n = 7), $HER2^+$ (n = 2), Triple negative (n = 3)], 2 melanoma patients, and 3 patients with pancreas adenocarcinomas was used to identify circulating tumor cells. Cells were plated on a poly-L-lysine–treated surface (fig. S8) and immediately fixed in 95% ethanol for at least 30 minutes at room temperature. In combination with the standard CTC-iChip process, we have seen this plating method to best preserve cell morphology to allow sensitive cytopathological analysis. Papanicolaou stain was done with hematoxylin, Eosin-Azure (EA), and Orange G. Slides were dehydrated and coverslipped with permanent mounting medium.

Immunocytochemistry

Coverslips of the Papanicolaou-stained slides were removed with xylene, and slides were rehydrated through ascending alcohols. Endogenous peroxidase activity was blocked by 0.03% hydrogen peroxide in methanol for 20 minutes. Antigen retrieval was performed for all immunostains (except HER2) by boiling slides in 10 mM citrate buffer (pH 6.0) for 20

minutes. An additional permeabilization step was required for the estrogen receptor (ER) immunostain, using 0.2% Triton X-100 in PBS for 10 minutes. Slides were incubated with primary antibody (table S3) for 60 minutes, followed by specific secondary anti-rabbit or anti-mouse immunoperoxidase polymers (EnVision+ System HRP Labelled Polymer, Dako) for 30 minutes. The labeled peroxidase was observed using Vector NovaRED, Vector DAB or Vector VIP peroxidase substrate kits (Vector Labs). After counterstaining slides with Gill's Hematoxylin (Vector labs) for 10 min, slides were dehydrated, cleared and permanently mounted using Shandon Mount (Thermo Scientific). All procedures were performed at room temperature and the slides were washed 3 times with PBS-Tween 0.1% before and after incubation of antibody. Cytospins of cultured cells from cell lines served as positive and negative controls (fig. S9).

Evaluation of Papanicolaou and immuncytochemistry stains

Papanicolaou stained slides were screened by a trained cytotechnologist and reviewed by a board certified cytopathologist. Cells were considered 'suspicious for malignancy' if the cells showed nuclei that were larger, more hyperchromatic and irregular compared to surrounding blood cells. Suspicious cells were photographed at 1000× original magnification with oil immersion Olympus microscope (Olympus, BX51), using Olympus DP25 camera and Adobe Twain software. Those cells or group of cells that were considered suspicious on review of the Pap-stained slides were re-visited after immunocytochemical staining and photographed again. Histopathological and cytological slides of primary and/or metastatic tumors of the same patients were retrieved from file of the pathology department for comparison of morphological and immunohistochemical features.

Quantitative cytopathology image analysis

Micrographs of individual CTCs and surrounding white blood cells taken at 100X magnification were imported into LabView for analysis. Image processing code was written to automatically generate particle measurements for each individual cell. Briefly, the saturation plane was extracted from the original image with a dilation filter subsequently applied (7×7 structuring element, single iteration). Following, a square look up table was applied and the resulting image was binarized by applying a manual threshold (set at the same constant value for all images). For all objects, particle measurements were obtained, including the maximum feret diameter, referred to as the "effective diameter" (Fig. 6). The maximum feret diameter represents the longest distance between any two points along the object's perimeter. For a cell to be identified as a CTC, it had to meet two criteria: (i) positive staining for a tumor specific marker by immunocytochemistry (e.g. cytokeratin, melanin-a), and (ii) positive scoring upon review by the cytopathologist (E.B.). White blood cells were identified based on their morphology, PAP staining, and cytopathologist score.

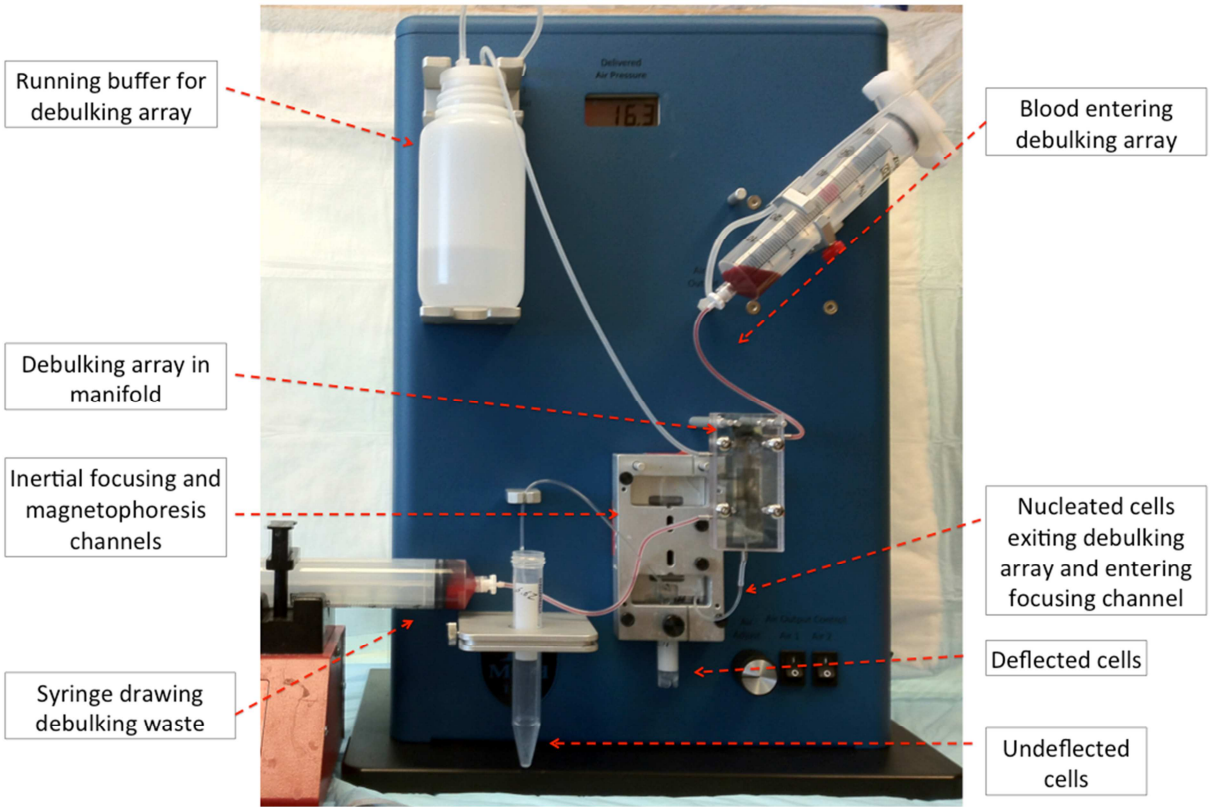

Figure S1. CTC-iChip system details. The overall system was driven by a pressure source that pushed the running buffer and whole blood into the debulking array. The waste outlet was connected to a syringe pump that withdraws the waste solution containing RBCs at a volumetric flow rate of 550 µl/min, approximately 4-fold greater than the array product flow rate of 140 µl/min. This ratio and the selected driving pressure (16-21 PSI) were used to ensure the purity of the array product and maintain the flow rate needed for optimal inertial focusing. The magnetically deflected cells were collected as they drip down from the edge of the device, while the undeflected cells were collected via exit tubing.

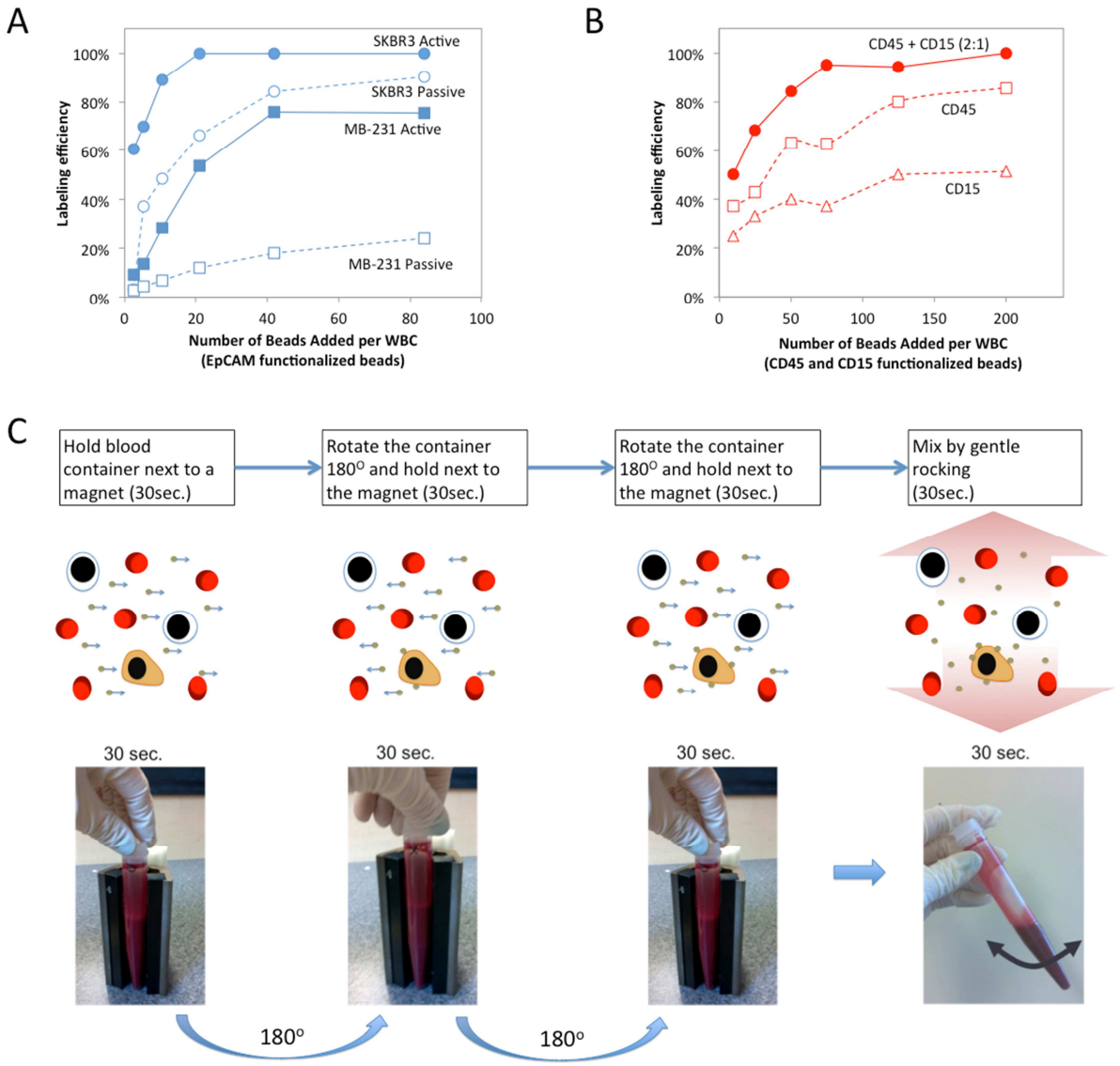

Figure S2. Optimization of labeling in whole blood. Labeling efficiency of target cells in whole blood was determined as a function of magnetic bead concentration and mixing strategies. (**A**) Labeling efficiency of target cells with anti-EpCAM–functionalized magnetic beads in positive selection mode. Active magnetic mixing was required to achieve high labeling efficiency of low EpCAM-expressing cells. Labeling efficiency corresponds to percent of target cells with magnetic bead loading sufficient to enable isolation in the positive selection device (15 beads). (**B**) Labeling efficiency of WBCs for negative depletion. Cells were labeled with anti-CD15 beads, anti-CD45 beads, or both. Labeling efficiency corresponds to percent of WBCs with magnetic bead loading sufficient to enable isolation in the negative depletion device (4 beads). (**C**) For positive selection, following the addition of magnetic beads into the specimen, active mixing was employed by bringing the sample tube in contact with a magnet, removing the magnet, rotating the tube, and bringing it back in contact with the magnet; this cycle was repeated 7 times.

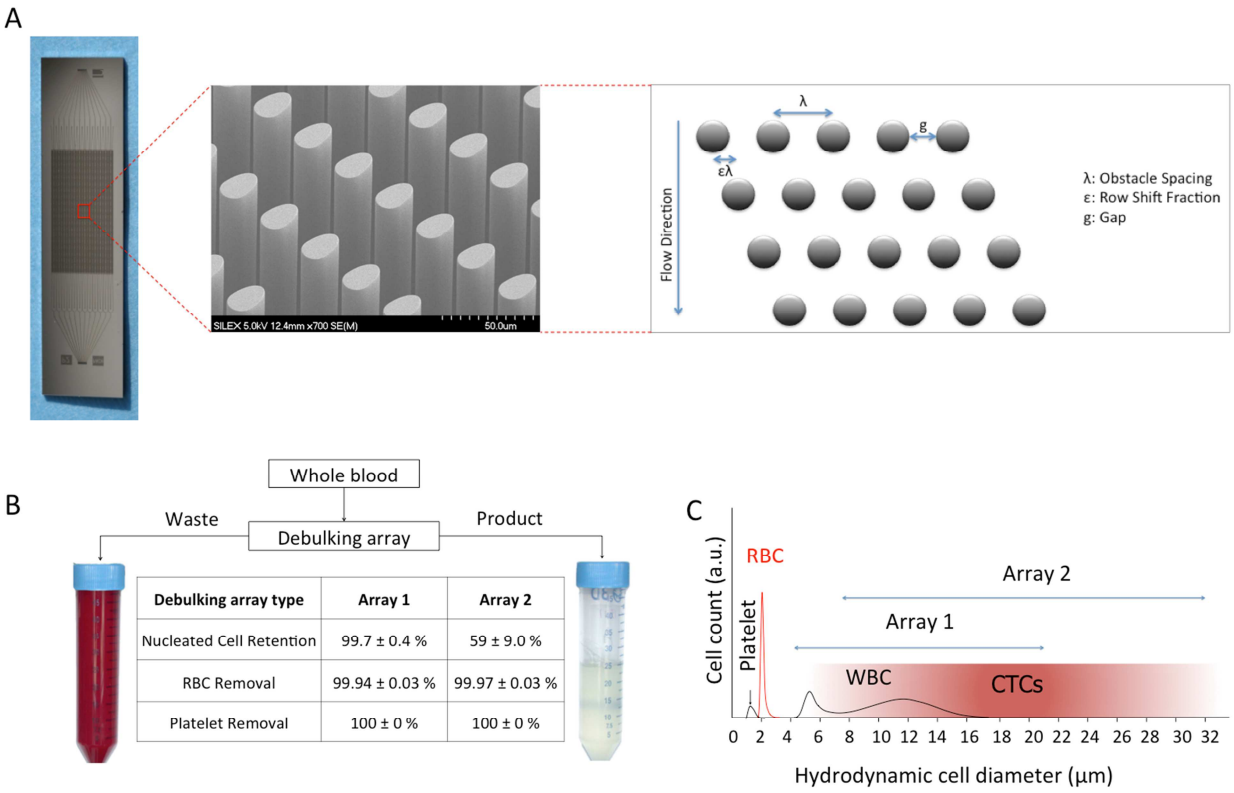

Debulking array type	Array 1	Array 2
Nucleated Cell Retention	99.7 ± 0.4 %	59 ± 9.0 %
RBC Removal	99.94 ± 0.03 %	99.97 ± 0.03 %
Platelet Removal	100 ± 0 %	100 ± 0 %

Figure S3. Hydrodynamic size–based separation. A single debulking array has 24 parallel channels and arrays are 150 µm in depth. Each of the 24 parallel channels has two input streams that run side-by-side in laminar flow. (**A**) Building on previously established design principles, we developed two different array configurations, Array 1 and Array 2. The gaps between posts (g) were 20 and 32 µm for Arrays 1 and 2, respectively. The center-to-center distances between the posts (λ) were 35 and 56 µm, respectively, and the row shift fraction (ε) was 0.16 for both array designs. (**B**) Cell retention and debulking efficiencies were characterized for both of the arrays in multiple experiments ($n > 10$). (**C**) In our current study, we measured CTC diameters between 8 and 20 µm (Fig. 6). Therefore, we estimated a lower size cut-off of 8 µm, and larger size range going up to 30 µm. We concluded that the approximated CTC size range overlaps best with Array 2.

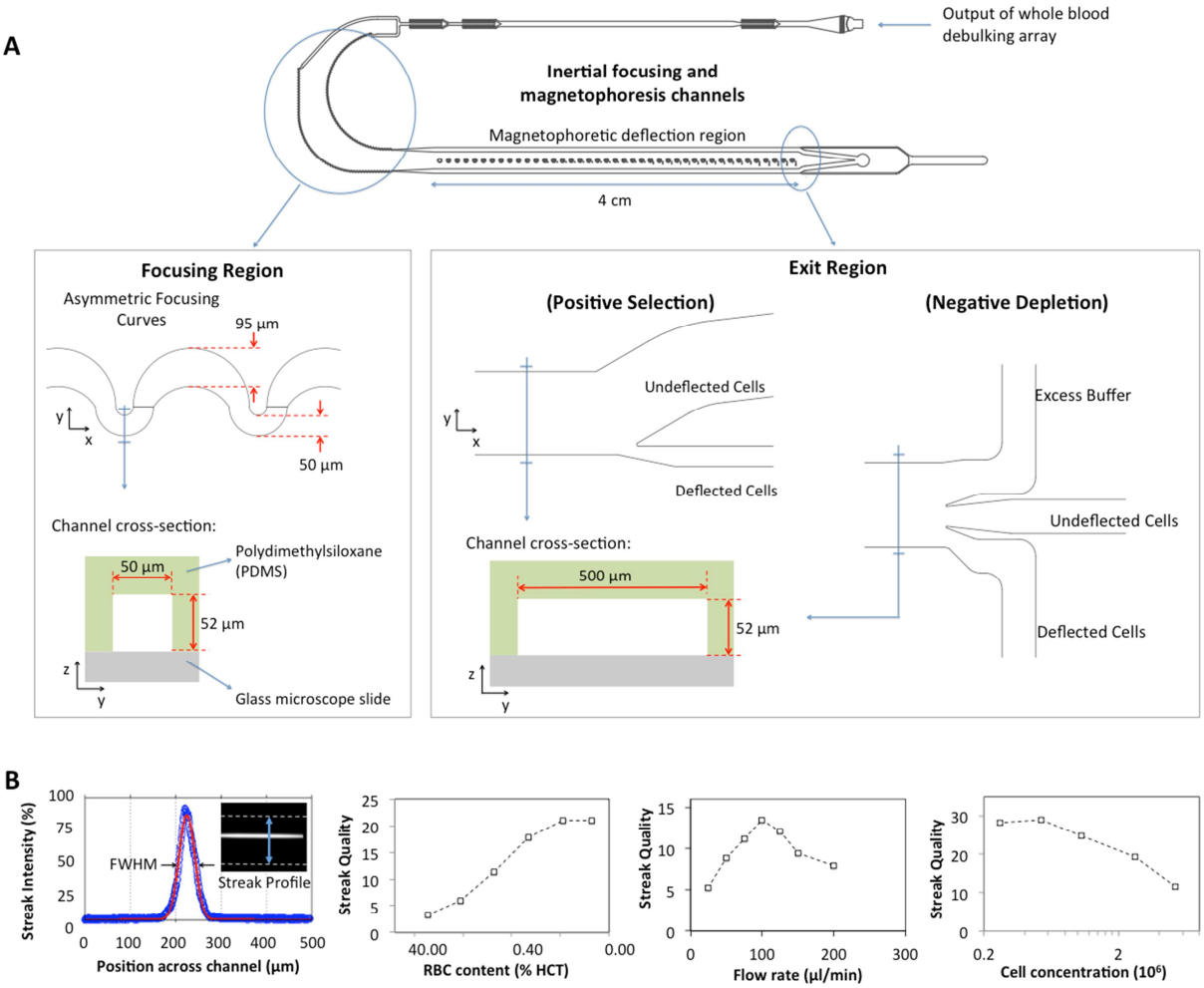

Figure S4. Inertial focusing and magnetophoresis channels. (**A**) Microfluidic channel layout and outlet configurations for positive selection and negative depletion. The channels were 52 µm high and consisted of 3 distinct regions: an inlet region with filters, a focusing region, and a magnetophoresis region. The inlet filters avoided downstream clogging of channels and had a gap size of 30 µm. The focusing region consisted of 60 asymmetric serpentine curves and a connecting curve. In the magnetophoresis region, the channel expanded to a 500 µm width. The number of outlets differs between the two modes to separate the deflected and undeflected cells at the end of the channel. Device throughput was doubled by multiplexing 2 channels. (**B**) Operating conditions were characterized by tracking the dependence of focused streak quality on flow rate, nucleated cell concentration, and contaminating RBCs. Focus quality was quantified by measuring the full-width-at-half-maximum (FWHM) of streak images of focused cells in the magnetophoretic deflection channel. Streak quality is channel width divided by measured FWHM of focused stream.

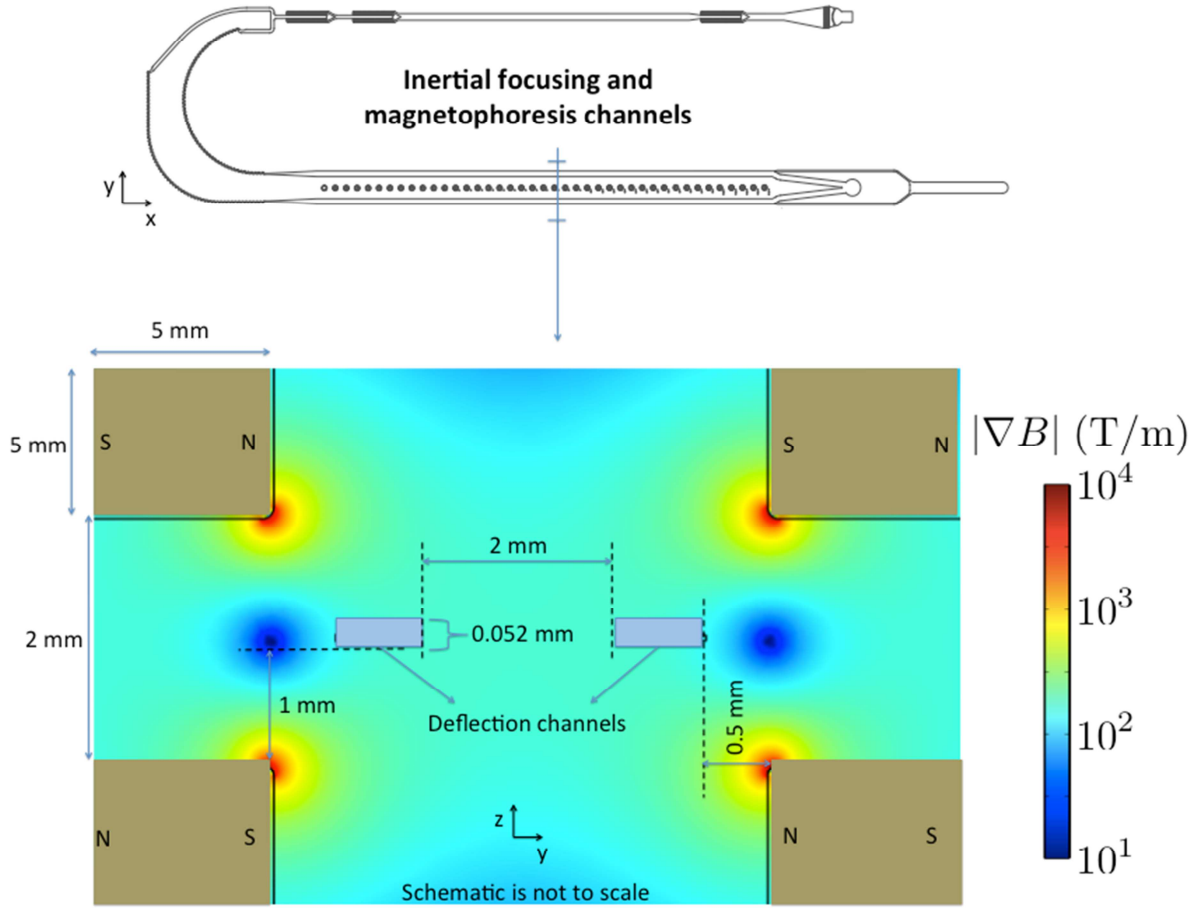

Figure S5. Magnetic configuration. The two magnetophoresis channels are shown in cross-section (gray). The four bar magnets that formed the quadrapole circuit are depicted at the corners (tan) and the resulting magnetic field gradient is shown. Stabilization screws on the manifold maintained alignment of the channels within the quadrapole magnetic circuit.

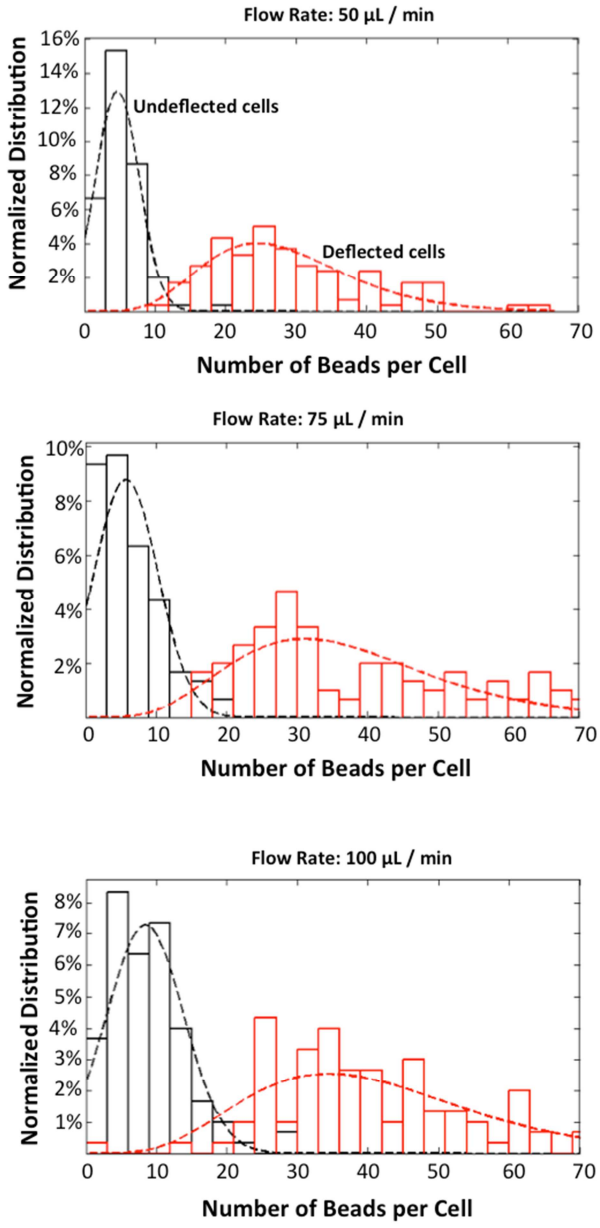

Figure S6. Beads per cell distribution in deflected and undeflected outputs. The distribution of beads per cell in the product and waste outlets from samples processed at 3 different flow rates are plotted in a fashion similar to that shown in Fig. 2C. Human prostate cancer cell line PC3-9 was used for this analysis. The intersection of the distributions in each of these three panels was used to plot the "minimum required magnetic load" in Fig. 2D. This experiment was performed in triplicate.

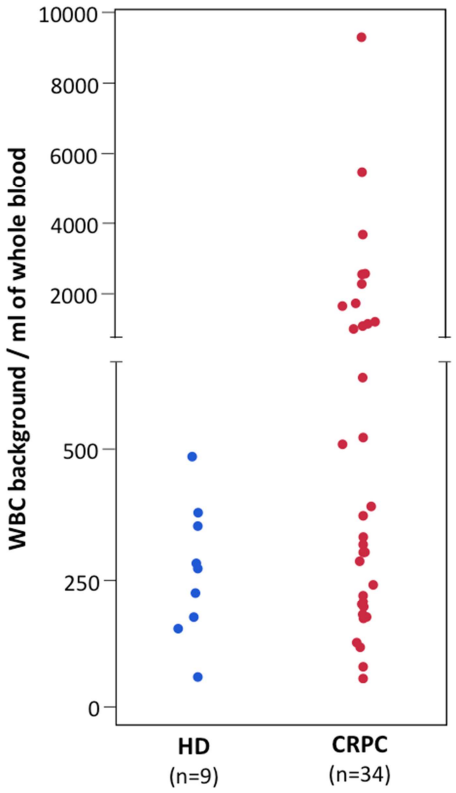

Figure S7. WBC contamination in ^{pos}CTC-iChip. The WBC contamination in the ^{pos}CTC-iChip product was characterized as a part of the study conducted on castration-resistant prostate cancer (CRPC) patients and on healthy donors. Number of WBCs is measured as total of DAPI-only and DAPI^{+}/CD45^{+} events on the scanned slide.

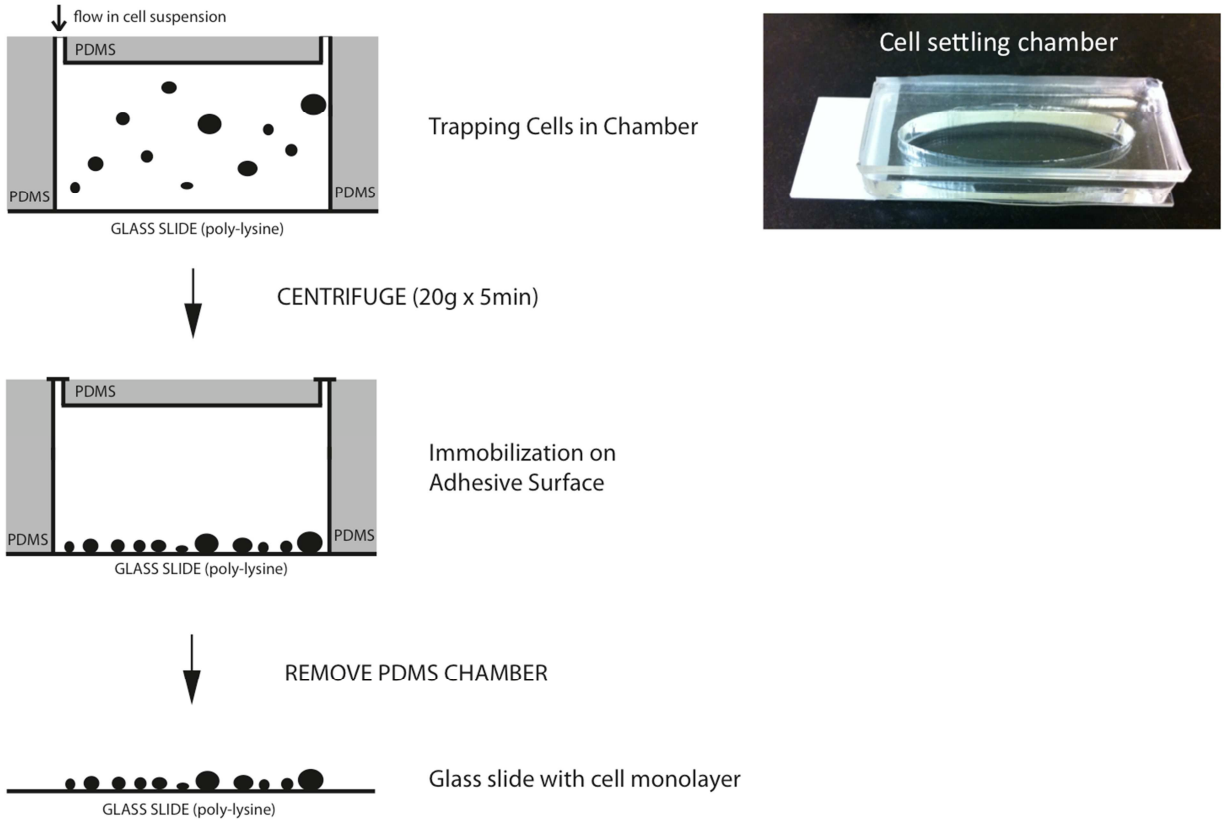

Figure S8. Cell plating chamber. To facilitate various cell staining and imaging methods, CTC-iChip products were plated on a glass surface. A simple PDMS chamber was fabricated and adhered to a clean glass surface. To promote cell adhesion, the chamber was treated with poly-L-lysine. The CTC-iChip product was loaded into the chamber and cells plated onto the glass surface via gentle centrifugation to speed up the settling. When cells were stained with immunofluorescent probes in suspension, the chamber was inverted after cell immobilization and the glass surface was scanned with an upright microscope. For the cytopathological stains, the chamber was removed for further processing and high resolution imaging after cell immobilization.

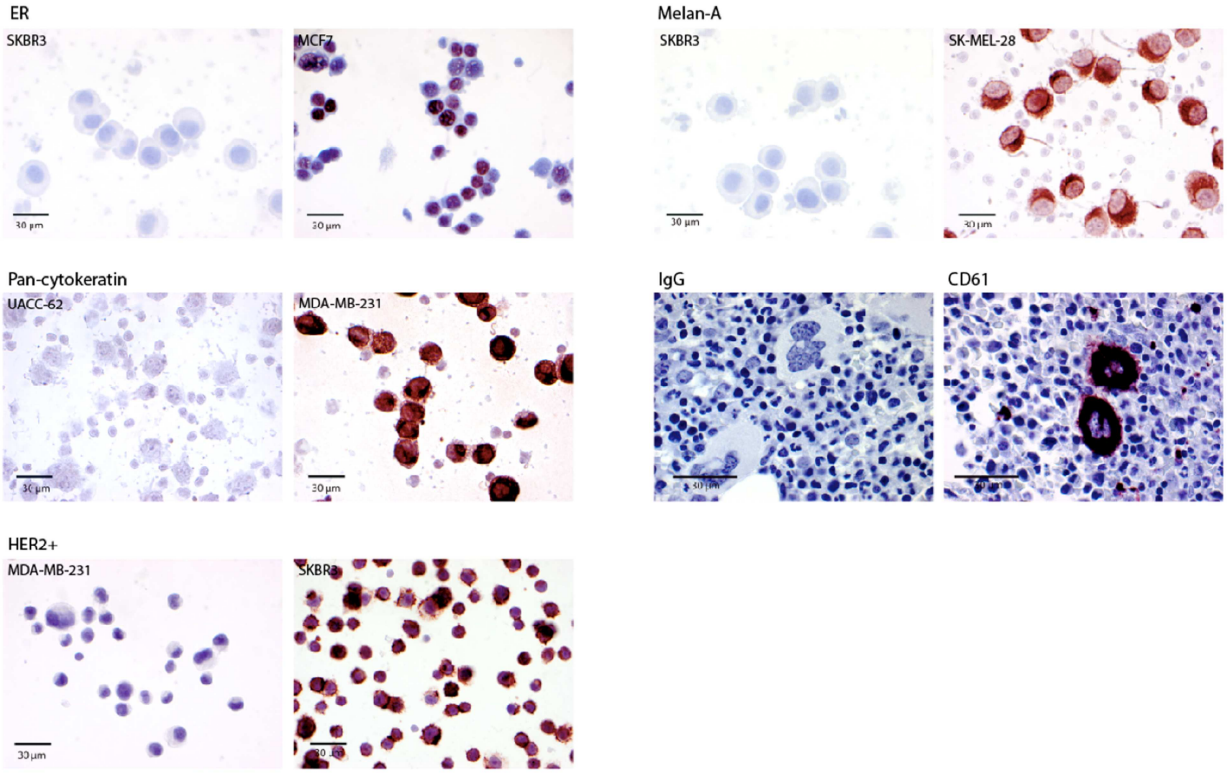

Figure S9. ICC stain validation through cell lines. The 5 ICC stains for ER, CK, HER2, Melan-A, and CD61 were validated using negative and positive controls (left and right panels for each marker, respectively). For the four tumor-specific stains (ER, Pan-cytokeratin, HER2, Melan-A), cancer cell lines were used for both controls. For the CD61 stain, an irrelevant IgG was used in place of the primary antibody for the negative control sample. Scale bars, 30 µm.

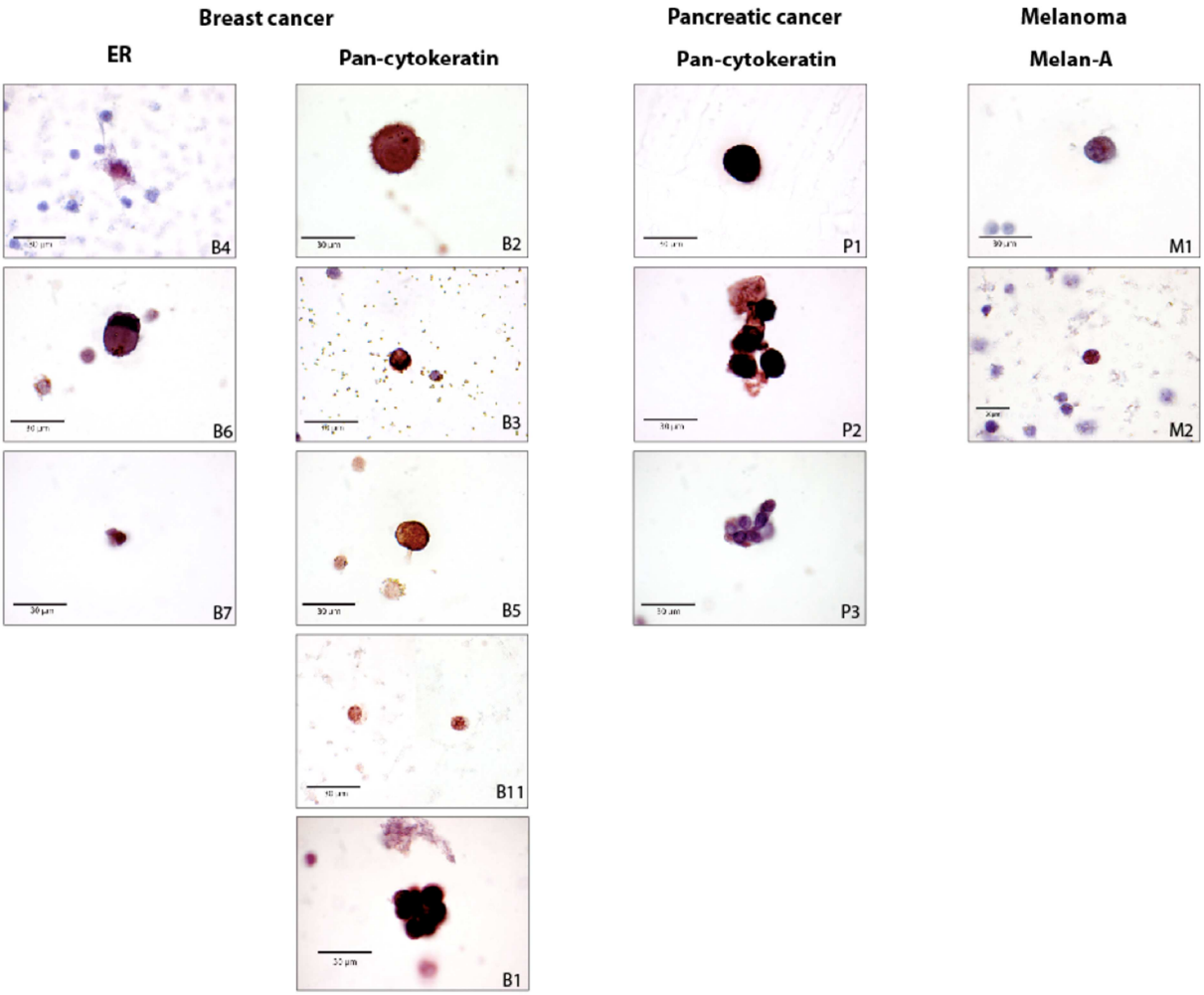

Figure S10. Additional images of ICC-stained cells. Thirteen additional CTCs observed to be positive for ICC stains similar to those presented in Fig. 5B. The variation in CTC size presented in Fig. 6 is also observed. Scale bars, 30 μm.

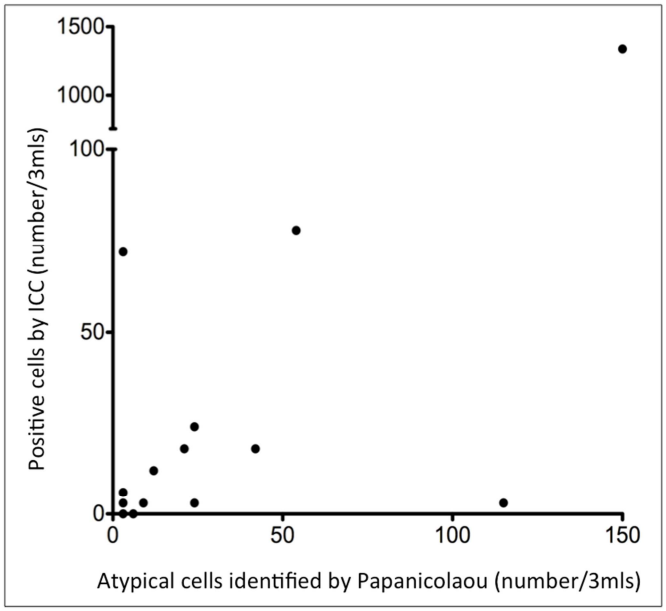

Figure S11. Comparison of cell identification through Pap and ICC. For each of 14 samples from cancer patients, the number of atypical cells identified by Pap staining and cells observed to be positive for a specific ICC marker is plotted.

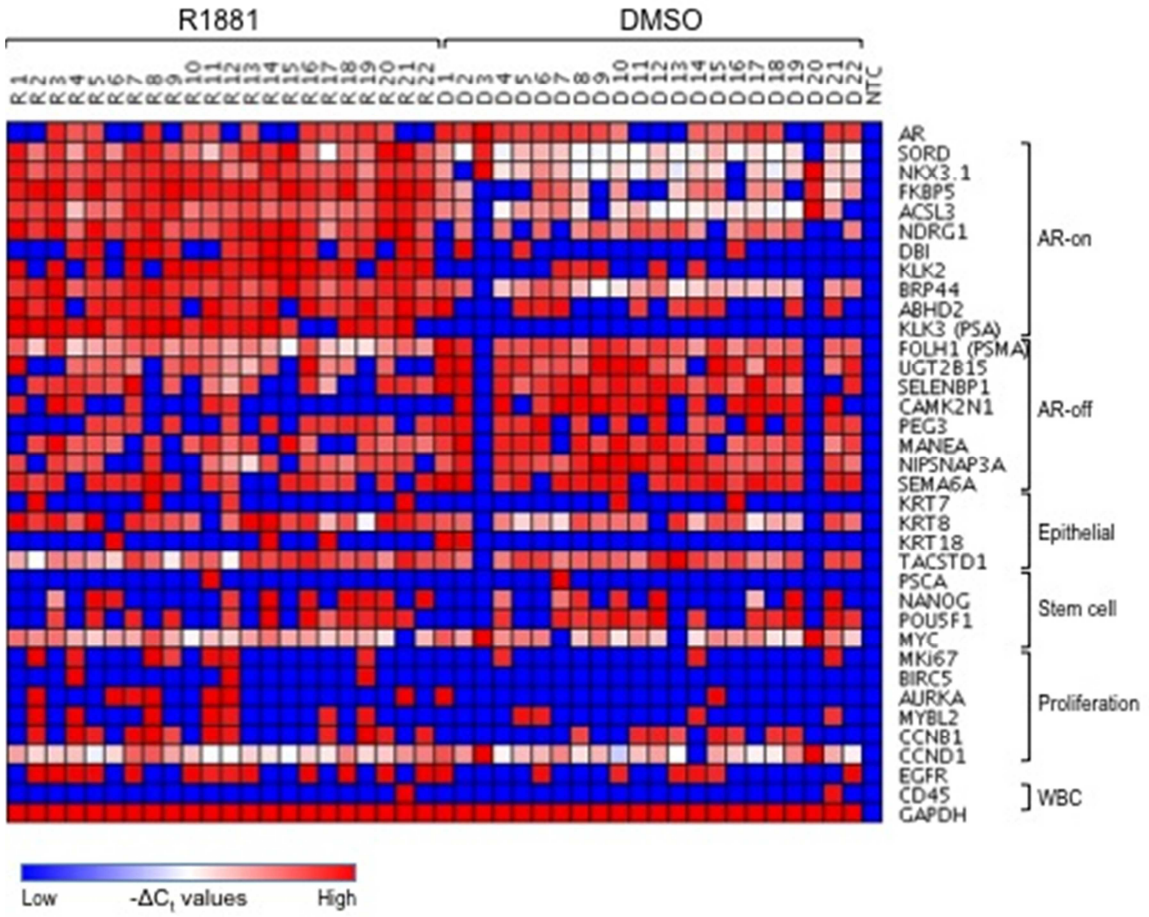

Figure S12. Single-cell qRT-PCR optimization using cell lines. Single cell transcriptional profiling of prostate cancer cells using microfluidic qRT-PCR. LNCaP cells were cultured under androgen-deprived conditions, treated for 24 h with 1 nM R1881 or DMSO, and then isolated for single cell expression analysis. Heat map displays normalized gene expression ($-\Delta C_t$) of a panel of genes in each of the single cells isolated. Columns list each individual cell, and rows show the genes assayed, grouped thematically.

SUPPLEMENTARY TABLES

Table S1. Contaminating cells in the ^{neg}CTC-iChip product are leukocytes. Flow cytometry analysis of the undeflected cells in ^{neg}CTC-iChip product was conducted to determine the fraction of cells that expressed CD45. Cells were stained using both a nuclear marker and anti-CD5 antibody. This analysis was performed for healthy donors (n = 5) and breast cancer patients (n = 4).

Sample	CD45$^+$ (%)
HD1	99.6
HD2	99.6
HD3	98.1
HD4	99.3
HD5	98.6
Patient1	99.0
Patient2	91.8
Patient3	98.0
Patient4	97.0
Average	**97.9**
Std. Dev.	**2.4**

Table S2. CellSearch versus ^{pos}CTC-iChip comparison. The number of CTCs found is shown for each of 42 patients. The volumes that were used for CTC-iChip process was not standardized, therefore variable recorded volumes needed normalization to standardized Veridex operation volume of 7.5 ml. A similar normalization was applied to CellSearch samples for which desired volume of blood was not acquired and system was operated with a smaller volume of blood.

Patient no.	Disease type	Number of cells per 7.5 ml		Total volume that was processed (ml)	
		CellSearch	CTC-iChip	CellSearch	CTC-iChip
1	Lung	1	0	7.5	3.5
2	Pancreas	0	0	7.5	6.7
3	Breast	0	0	7	7.8
4	Prostate	2	0	7.5	7.9
5	Pancreas	0	0	7.5	5.8
6	Prostate	1	1.0	7.5	6.9
7	Breast	0	1	7.5	7.3
8	Prostate	2	1.2	7.5	6.4
9	Pancreas	0	1.7	7.5	4.3
10	Breast	0	1.7	7.5	9.1
11	Prostate	1.7	1.8	4.5	8.4
12	Breast	1	2	7.5	7.7
13	Colorectal	0	2.1	7.5	7.3
14	Breast	2	2.3	7.5	6.5
15	Breast	0	2.7	7.5	5.5
16	Breast	1	3.2	7.5	7.1
17	Prostate	0	3.6	7.5	8.2
18	Prostate	9	4.1	7.5	7.2
19	Pancreas	0	5.3	7.5	5.7
20	Prostate	0	7.3	7.5	7.2
21	Breast	3	7.4	7.5	6.1
22	Colorectal	1	7.9	7.5	2.9
23	Prostate	0	8.1	7.5	3.7
24	Breast	10	8.2	7.5	7.4
25	Prostate	3	8.4	7.5	3.6
26	Prostate	1	8.7	7.5	3.4
27	Lung	4	9.1	7.5	4.2
28	Pancreas	7	9.1	7.5	4.9
29	Pancreas	0	10.5	7.5	3.6
30	Breast	5	10.6	7.5	7.1
31	Prostate	1	11.6	7.5	3.2

32	Prostate	1	14.5	7.5	2.6
33	Prostate	4	15.0	7.5	6.1
34	Breast	2	17.5	7.5	6.4
35	Prostate	6	24.2	7.5	5.9
36	Breast	23.1	27.4	6.5	7.7
37	Prostate	76	76.3	7.5	2.6
38	Prostate	238	230.8	7.5	3.5
39	Prostate	238	239.1	7.5	5.5
40	Prostate	334	326.4	7.5	2.8
41	Prostate	384	345.6	7.5	5
42	Prostate	4533	4579	7.5	6.4

Table S3. Antibodies used throughout the study.

Capture antibodies				
Target antigen	**Clone, isotype**	**Source**	**Use**	
EpCAM	VU-1D9, mouse monoclonal IgG1	Veridex LLC	Cell line capture, clinical samples	
EpCAM	Polyclonal goat IgG	R&D Biosystems, BAF960	Cell line capture, flow cytometry	
CD45	2D1, mouse monoclonal IgG1	R&D Systems, BAM1430	Cell line capture, clinical samples	
CD15	ICRF-29-2, mouse monoclonal IgM	R&D Systems, MAB7368	Cell line capture, clinical samples	
Antibodies used for ICC and IHC staining of ^{neg}CTC-iChip product				
Target antigen	**Clone**	**Dilution**	**Source**	**Antigen retrieval**
ER	NCL-L-ER 6F11	1:100	Leica	Citrate buffer, pH 6
HER2	c-erbB-2 (SP3)	1:100	Thermo Scientific	-
Pan-cytokeratin	AE1/AE3	1:200	AbCAM	Citrate buffer, pH 6
Melan-A	Melan-A (A103)	1:100	Santa Cruz	Citrate buffer, pH 6
CD61	CD61 Ab-1 (2F2)	Ready to use	Neomarkers	Citrate buffer, pH 6
Antibodies used for in-solution staining of ^{neg}CTC-iChip product prior to single-cell manipulation				
Target antigen	**Clone, isotype**	**Concentration or dilution**	**Source**	**Use**
EpCAM	VU-1D9, mouse monoclonal IgG1	1:50 (final concentration 4 µg/ml)	Cell Signaling Technologies (cat #: 2929)	Alexa Fluor 488 stain
CD45	HI30, mouse monoclonal IgG1	1:20	BD Biosciences (cat #: 562279)	PE-CF594 stain
Antibodies used for PSA/PSMA staining of ^{pos}CTC-iChip product				
Target antigen	**Clone, isotype**	**Concentraiton or dilution**	**Source**	**Use**
CD45	Polyclonal mouse IgG2a	1:500	Abcam C/N ab30470	IF staining primary
PSMA	J591, monoclonal mouse IgG1	10 µg/ml	Dr. N. Bander (Weill Medical College, New York)	IF staining primary
PSA	Polyclonal rabbit IgG	1:750	Dako C/N A0562	IF staining primary
Anti-mouse	Polyclonal goat IgG	1:500	Invitrogen C/N A21131	IF secondary, Alexa488

IgG2a Anti-mouse IgG1	Polyclonal goat IgG	1:500	Invitrogen C/N A21127	IF secondary, Alexa555
Anti-rabbit IgG	Polyclonal goat IgG	1:200	Jackson ImRes. C/N 111-495-144	IF secondary, DyLight 649

Antibodies used for CK staining of ^{pos}CTC-iChip product

Target antigen	Clone, isotype	Concentration (µg/ml)	Source	Use
CK8/18	C11, mouse monoclonal IgG1	2.4	Veridex LLC	IF stain, conjugated to PE
CK 19	A53-B/A2, mouse monoclonal IgG2a	2.4	Veridex LLC	IF stain, conjugated to PE
CD45	HI30, mouse monoclonal IgG1	10	Veridex LLC	IF stain, conjugated to APC